Site-specific atomic ordering in Pt-based high-entropy alloy for enhanced methanol oxidation

Guangtao Mao[a], Xiyue Han[a], Yuan Xiong[a], Leqing Luo[a], Zhouxun Zeng[a] and Qingmei Wang*[abc]

[a] School of Chemistry and Chemical Engineering, Guizhou University, Guiyang, Guizhou, 550025, China

[b] Guizhou Provincial Key Laboratory of Green Chemical and Clean Energy Technology, Guiyang, Guizhou, 550025, China

[c] Guizhou Provincial Key Laboratory of Green Catalysis and Materials for resource conversion, Guiyang, Guizhou, 550025, China

Supplementary Material

Physical characterization

X-ray diffraction patterns were collected on a Bruker X-ray diffractometer (model D8 ADVANCE) using Cu Kα radiation and a scan rate of 5°min^{-1}. Transmission electron microscopy (TEM) and high-resolution transmission electron microscopy (HRTEM) images were obtained on a Tecnai TF20 operated at an acceleration voltage of 200 kV. High-angle annular dark-field scanning transmission electron microscopy (HAADF-STEM) and energy dispersive X-ray spectroscopy (EDS) analyses were performed on a Chen-Sheng OPtics SC-LX41M operating at 200 kV with a cold field-emission gun and aberration corrector. The N_2 adsorPtion–desorPtion isotherms were measured using a BSD-PM2 gas adsorPtion analyzer to determine the specific surface area and average pore size distribution of materials. X-ray photoelectron spectroscopy (XPS) data were collected on a Shimadzu SGLC-Axis Supra spectrometer. All the peaks were adjusted using the C 1s peak at 284.8 eV as the reference. The ultraviolet photoemission spectroscopy (UPS) data of the samples were obtained using a PHI 5000 Versaprobe III with an He I ultraviolet light. The ICP-OES analysis was manipulated on an Elan

DRC-e instrument. In situ Fourier transformed infrared (FTIR) spectra were collected on a Thermo Scientific Nicolet 6700 FT-IR spectrometer equipped with attenuated total reflection (ATR) configuration using a liquid nitrogen cooled MCT-A detector.

Sample Preparation for Physical Characterization

XRD: Powder samples were ground finely in an agate mortar to ensure uniform particle size. Approximately 20 mg of the ground sample was loaded onto a zero-background silicon sample holder, carefully flattened with a glass slide to create a smooth, even surface, and gently pressed to avoid preferential orientation effects. The prepared holder was then immediately transferred to the diffractometer for measurement.

Microscopy (TEM/STEM): Approximately 1 mg of catalyst powder was dispersed in 5 mL of ethanol by ultrasonication for 15-20 minutes to obtain a homogeneous suspension. A drop of the suspension (about 5-10 μL) was then carefully deposited onto a holey carbon-coated copper grid (200 mesh) using a micropipette. The grid was placed on filter paper to absorb excess liquid and dried under ambient conditions for at least 2 hours before insertion into the microscope column.

N_2 Adsorption: Approximately 50-100 mg of sample was accurately weighed and placed into a glass analysis tube. The tube was attached to the degassing port and heated at 200 °C under vacuum (10^{-3} Torr) for 6-8 hours to remove any adsorbed moisture or volatile impurities. After degassing, the tube was backfilled with nitrogen, transferred to the analysis port, and nitrogen adsorption-desorption isotherms were measured at 77 K using liquid nitrogen as coolant.

XPS: Powder samples were pressed onto double-sided carbon tape adhered to a stainless steel sample holder, ensuring complete coverage of the tape surface. The prepared holder was then introduced into the spectrometer's load lock chamber and degassed under high vacuum (10^{-6} Torr) for 2 hours to remove volatile contaminants before transferring to the analysis chamber for measurement.

UPS: Sample preparation followed the same procedure as XPS. Additionally, to obtain clean surfaces representative of the bulk material, samples were subjected to gentle argon ion etching (1 kV, 1 μA, for 2 minutes) inside the preparation chamber to remove any surface adventitious carbon or adsorbed species before UPS analysis.

In situ FTIR: The working electrode was prepared by drop-casting the catalyst ink onto a glassy carbon disk electrode and drying under ambient conditions. A custom-built spectroelectrochemical cell equipped with a CaF_2 prism as the IR window was used, with the working electrode pressed against the prism to create a thin-layer configuration. The cell was assembled with the catalyst-modified electrode, a platinum wire counter electrode, and an Ag/AgCl reference electrode, then connected to the potentiostat and FTIR spectrometer. Electrolyte (0.1 M $HClO_4$ + 0.5 M CH_3OH) was introduced, and spectra were collected during potential steps while maintaining optical alignment. The in situ FTIR measurements were performed on a Thermo Scientific Nicolet 6700 FT-IR spectrometer equipped with a liquid nitrogen-cooled MCT-A detector and an attenuated total reflection (ATR) configuration. A custom-built spectroelectrochemical cell was used, featuring a CaF_2 prism as the IR window at the bottom. The working electrode was a thin Pt-HEA-6/HMCSs catalyst film deposited on a glassy carbon disk, the counter electrode was a platinum wire, and the reference electrode was Ag/AgCl (3 M KCl). All potentials were converted to the RHE scale. Spectra were collected during potential steps from 0.1 V to 1.0 V vs. RHE in N_2-saturated 0.1 M $HClO_4$ containing 0.5 M CH_3OH. Each spectrum was acquired by accumulating 32 interferograms with a spectral resolution of 4 cm^{-1}. The background spectrum was collected at 0.1 V vs. RHE before methanol oxidation.

ICP-OES: Approximately 10 mg of sample was accurately weighed and transferred to a PTFE digestion vessel. Freshly prepared aqua regia (3:1 HCl/HNO_3, 5 mL) was added, and the vessel was sealed and heated at 80 °C on a hot plate for 2 hours with occasional swirling to ensure complete digestion. After cooling to room temperature, the digested solution was quantitatively transferred to a 50 mL volumetric flask and diluted to the mark with 2% HNO_3. The solution was filtered through a 0.22 μm syringe filter before analysis to remove any undigested carbon residues. Each sample was prepared in triplicate for statistical reliability.

Reference electrode calibration

The reference electrode (Ag/AgCl in 3 M KCl) was calibrated against a reversible

hydrogen electrode (RHE) in the same electrolyte (0.1 M $HClO_4$) prior to all measurements. The calibration was performed in a standard three-electrode cell using a platinum wire as the working electrode and a platinum plate as the counter electrode. High-purity hydrogen gas was bubbled into the electrolyte to saturate the solution, and the open circuit potential between the Ag/AgCl reference electrode and the platinum wire (which acts as a reversible hydrogen electrode under these conditions) was recorded. The measured potential was stable at +0.222 V vs. RHE. All potentials reported in this work were converted to the RHE scale using the equation: E (V vs. RHE) = E (V vs. Ag/AgCl) + 0.222 V.

Electrochemical measurements

Electrochemical measurements were performed in a three-electrode cell interfaced with an electrochemical workstation (Dong-Hua DH7000). A graphite rod and an Ag/AgCl (3 M KCl) electrode were adoPted as the counter and reference electrodes, respectively. The reference electrode was corrected to a reversible hydrogen electrode (RHE) in the identical electrolyte before measurements. The working electrodes were prepared by applying catalysts inks onto glassy carbon (GC) disk electrodes. The working electrode was a glassy carbon disk electrode with a geometric area of 0.19625 cm^2 (diameter: 5 mm). Catalyst inks were prepared by dispersing the catalyst (2 mg) in a mixed solution containing 5 uL of 5 wt.% Nafion solution and 800 uL of ethanol under sonication for a minimum of 30 min. Then, 12 uL of a homogeneous catalyst ink was then pipetted onto the GC surface. After drying in air at room temperature, a drop of a 0.01 wt.% Nafion solution was applied on the top surface of the catalyst layer and the resulting modified electrode dried in air at room temperature. A commercial Pt/C catalyst (E-TEK, 20 wt. % Pt, Pt particle size: 2-5 nm) was used in this work as a benchmark AOR catalyst. The electrolyte was “not stirred” during any of the electrochemical measurements, including cyclic voltammetry, CO stripping, chronoamperometry, and accelerated durability tests. All experiments were conducted under static conditions to ensure consistent mass transport conditions and avoid forced convection that could affect the reaction kinetics.

The MOR measurements were performed in a potential range of 0.05 to 1.2 V vs. RHE, which corresponds to approximately -0.17 to 0.98 V vs. Ag/AgCl in 0.1 M $HClO_4$. The CO stripping experiments were conducted from 0.05 to 1.2 V vs. RHE (-0.17 to 0.98 V vs. Ag/AgCl). The chronoamperometry tests were performed at 0.75 V vs. RHE (0.53 V vs. Ag/AgCl). All potential conversions were calculated using the calibrated value of E(RHE) = E(Ag/AgCl) + 0.222 V in 0.1 M $HClO_4$. Before electrochemical measurements, all the electrodes were pre-conditioned by cycling the potential between 0.05 V and 1.2 V vs. RHE at a scan rate of 50 mV s^{-1} for 100 cycles to remove any surface impurities.

The onset potential for methanol oxidation reaction (MOR) is defined as the potential at which the oxidation current density reaches 0.1 $mA \cdot cm^{-2}$, after subtracting the background current measured in the absence of methanol. This value was consistently applied to all catalysts to enable fair comparison. The onset potentials were extracted from the forward scan of the cyclic voltammograms recorded in N_2-saturated 0.1 M $HClO_4$ containing 0.5 M CH_3OH at a scan rate of 50 $mV \cdot s^{-1}$. The background current was obtained from CV scans in the same electrolyte without methanol. For each catalyst, the onset potential was determined using the electrochemical workstation software by identifying the potential corresponding to the threshold current density.

The alcohol oxidation reactions (AORs) tests were conducted in a N_2-saturated 0.1 M $HClO_4$ solution containing 0.5 M methanol (ethanol) at room temperature. The CO stripping experiments were performed in a 0.1 M $HClO_4$ electrolyte. CO gas was bubbled into electrolyte for about 20 min. Then the CO feed was replaced by a high-purity N_2 feed for 0.5 h. Chronoamperometry was performed at a potential of 0.75 V (vs. RHE) in 0.1 M $HClO_4$ + 0.5 M CH_3OH (CH_3CH_2OH) solution for 2000 s. The accelerated durability tests (ADT) were conducted by consecutive cyclic voltammetry scans in N_2-saturated 0.1 M $HClO_4$ containing 0.5 M CH_3OH at a scan rate of 50 $mV \cdot s^{-1}$, cycling between 0.05 and 1.2 V vs. RHE for 800 (or 5000) cycles. The durability was evaluated by comparing the final CV curve after the specified cycles with the initial one.

The electrochemical surface area (ECSA), mass activity and specific activity of the

catalysts were calculated using the following equation:

$ECSA = Q_{CO}/(0.42\times[Pt])$

where Q_{CO} is the charge associated with the integrated area of the CO dissolved peak; 0.42 mC cm_{Pt}^{-2} is the electrical charge parameter related to monolayer adsorPtion of hydrogen on Pt; [Pt] (mg) is the amount of Pt on the working electrode.

Lattice contraction and strain by XRD

The lattice contraction and strain in the MOAs were calculated using the Debye-Scherrer equation, specifically the following equation:

$L = 1/2d$

where L is the lattice parameter and d represents the interplanar spacing of a selected crystal plane. Here we selected the (111) crystal plane for lattice contraction and strain analyses, since the (111) reflection of the MOA NPs was the most intense in the XRD patterns of all the catalysts.

$L_2\ strain\% = (L_1-L_2)/L_1$

where L_2% is the percentage change of the lattice parameter of MOA NPs compared to a standard sample (Pt/C in this case), L_1 represents the lattice parameter of the Pt/C, and L_2 is the lattice parameter of the MOA samples.

Supplementary figures

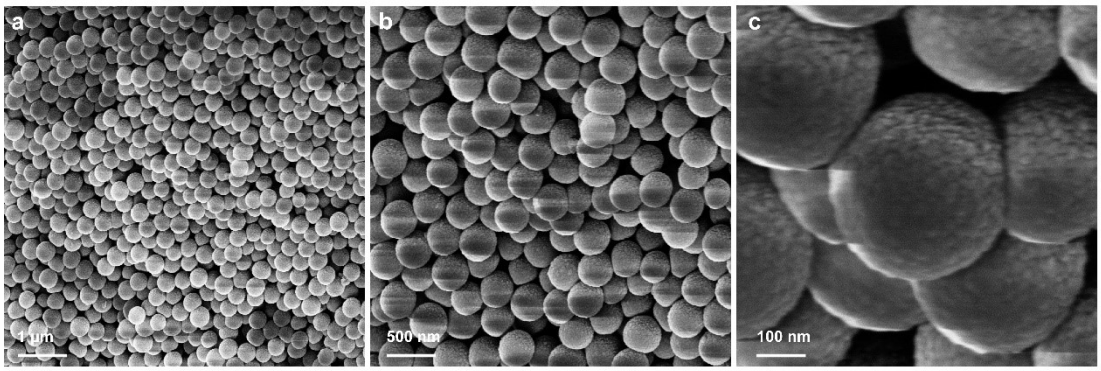

Figure S1. The SEM images of SiO_2@SiO_2/RF composite, (a) 1 μm, (b) 500 nm, (c) 100 nm.

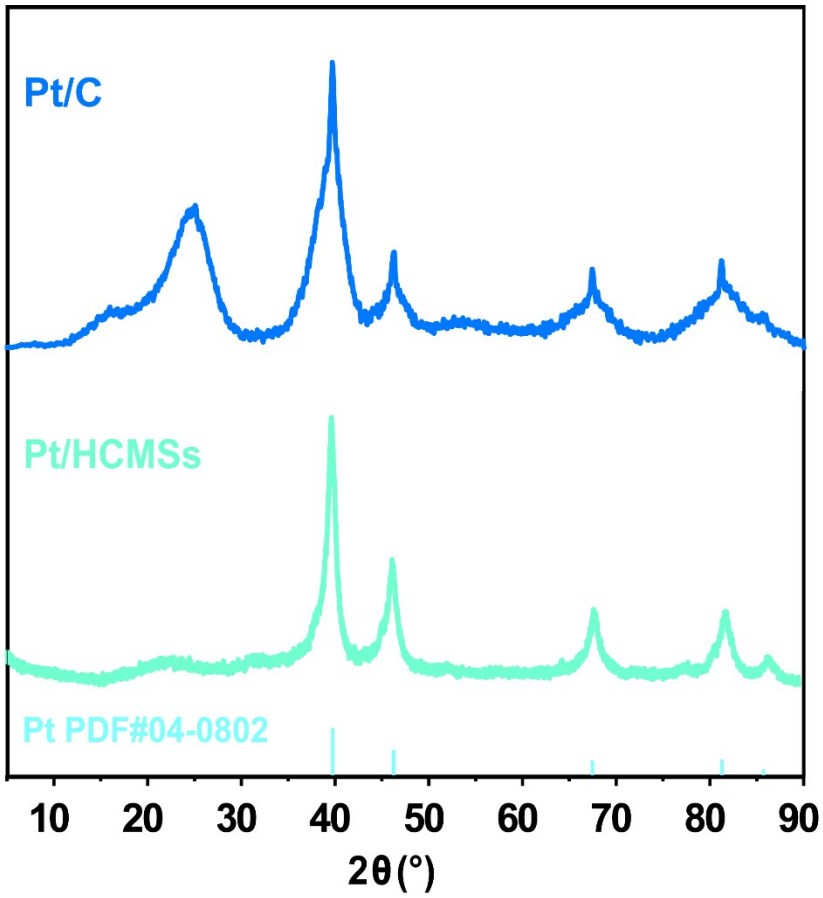

Figure S2. The XRD patterns of Pt/C and Pt/HMCSs.

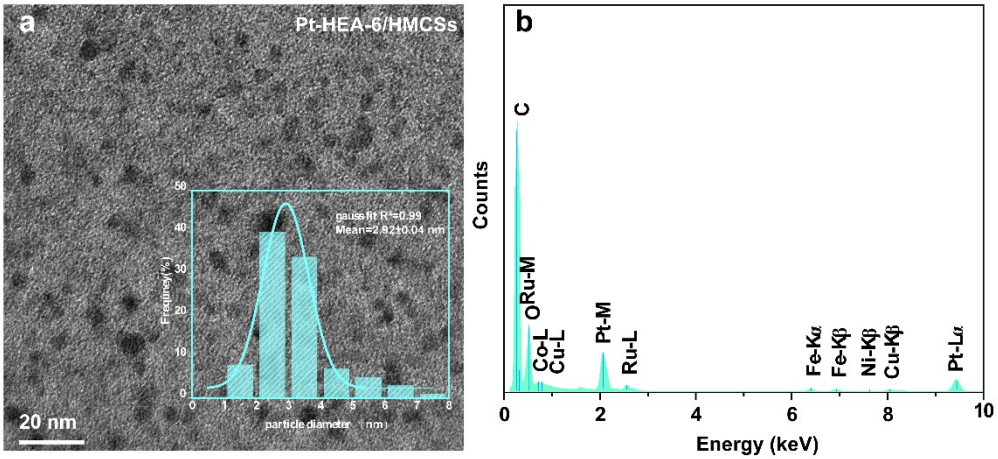

Figure S3. (a) TEM images and corresponding Pt nanoparticle size distributions for the Pt-HEA-6/HMCSs catalyst. (b) The atomic fraction of the Pt-HEA-6/HMCSs catalyst from EDX.

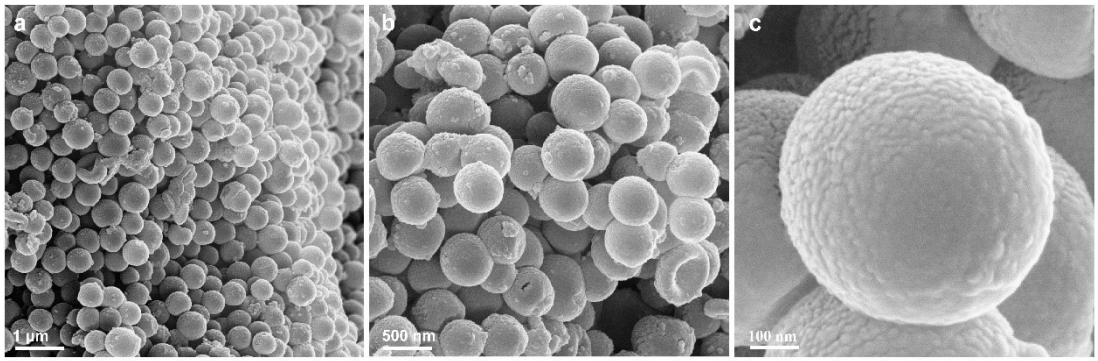

Figure S4. The SEM images of Pt-6-HEA/HMCSs composite (SiO_2@SiO_2/RF adsorbs metal cations and then carbonizes and reduces in a N_2/H_2 atmosphere), (a) 1

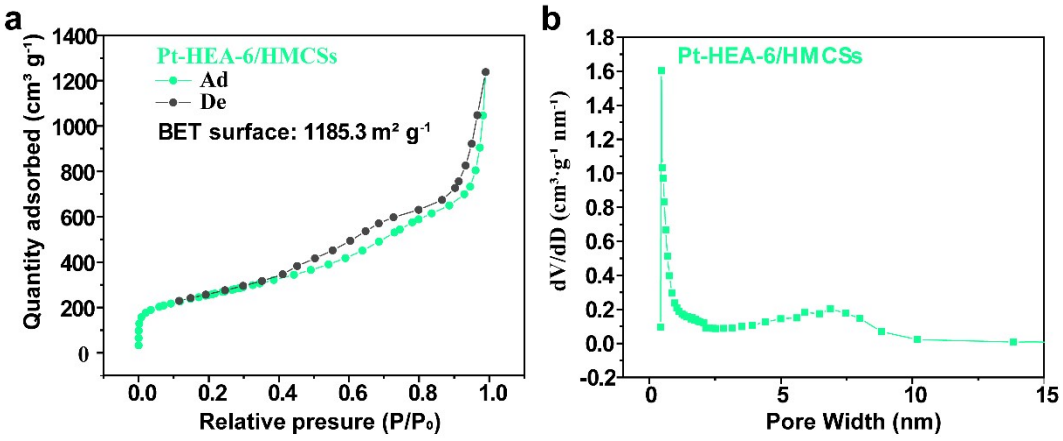

μm, (b) 500 nm, (c) 100 nm.

Figure S5. (a) N_2 adsorPtion-desorPtion isotherms and (b) pore size distribution and pore distribution curves of Pt-6-HEA/HMCSs.

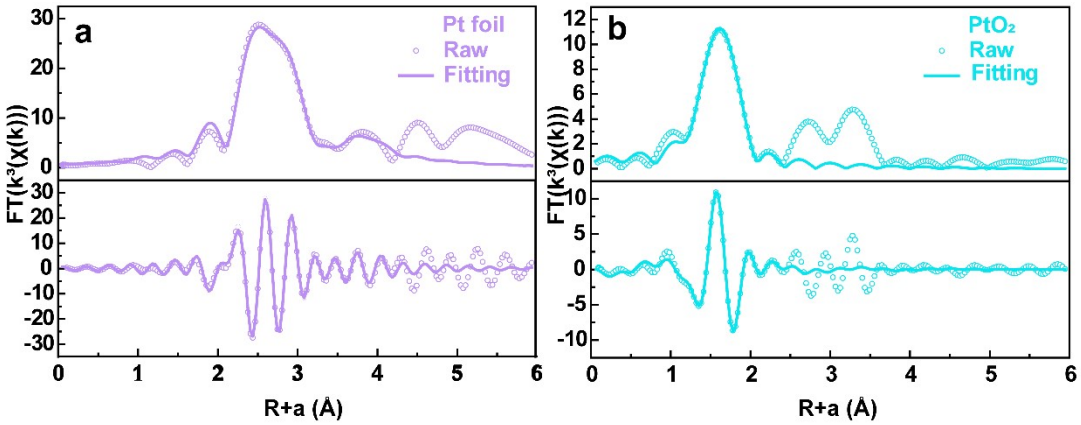

Figure S6. The EXAFS fitting curve Pt L_3-edge of Pt foil (a) and PtO_2 (b) at R-space.

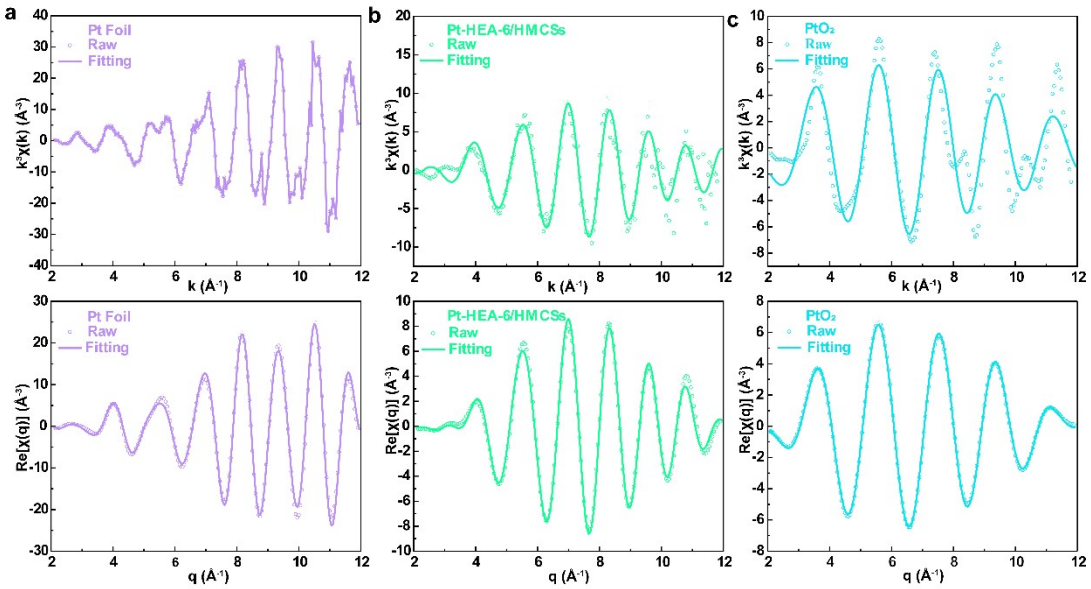

Figure S7. Pt L3-edge EXAFS (points) and curve-fit (line) for (a)Pt foil; (b) Pt-HEA-6/HMCSs and (c) PtO_2 shown in k3-weighted k-space. Pt L3-edge EXAFS (points) curve-fit (line) (d)Pt foil; (e) Pt-HEA-6/HMCSs and (f) PtO_2 shown in k3-weighted in inverse FT-EXAFS.

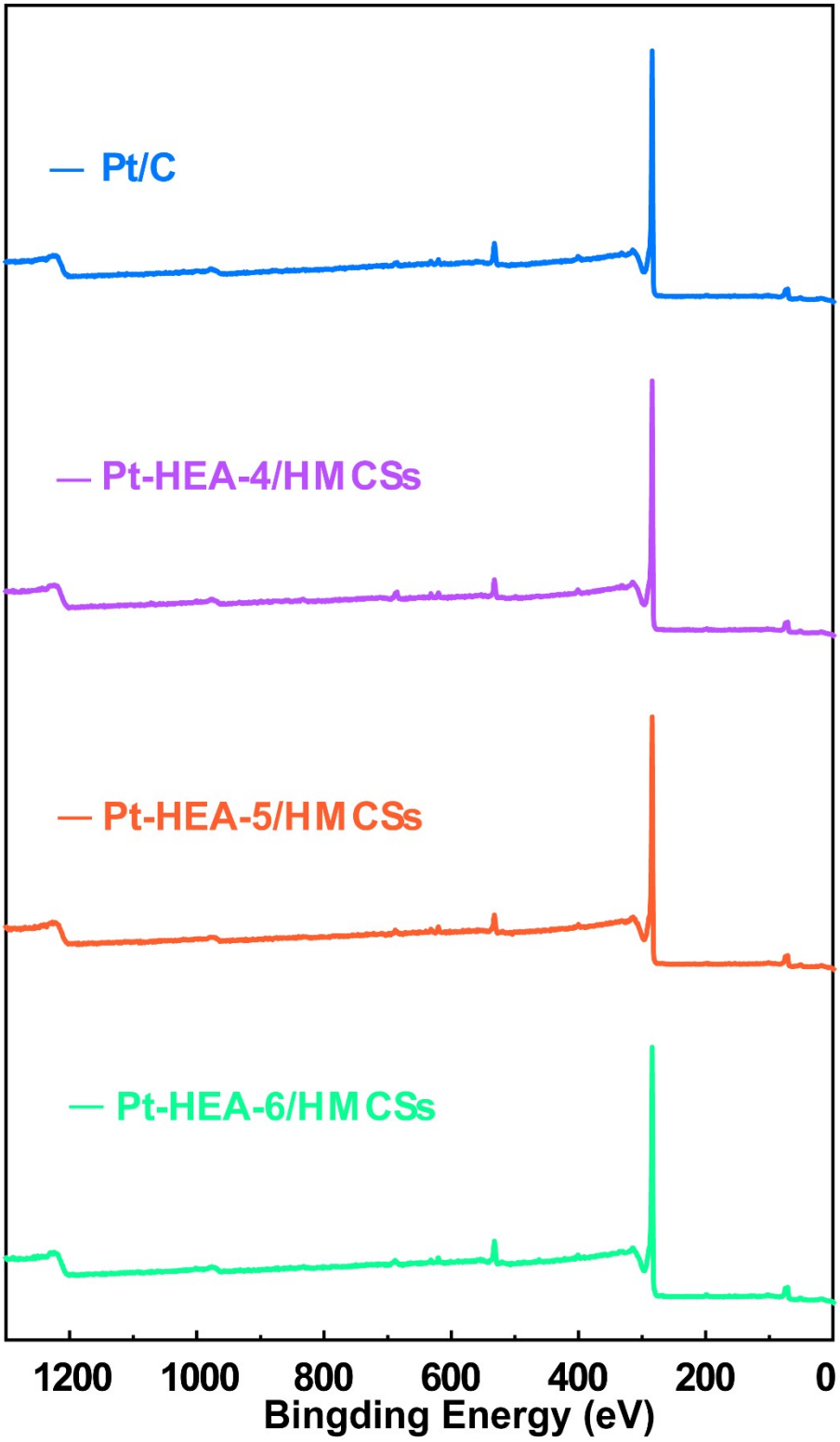

Figure S8. The XPS survey spectrum of commercial Pt/C, Pt-HEA-4/HMCSs, Pt-HEA-5/HMCSs and Pt-HEA-6/HMCSs catalysts.

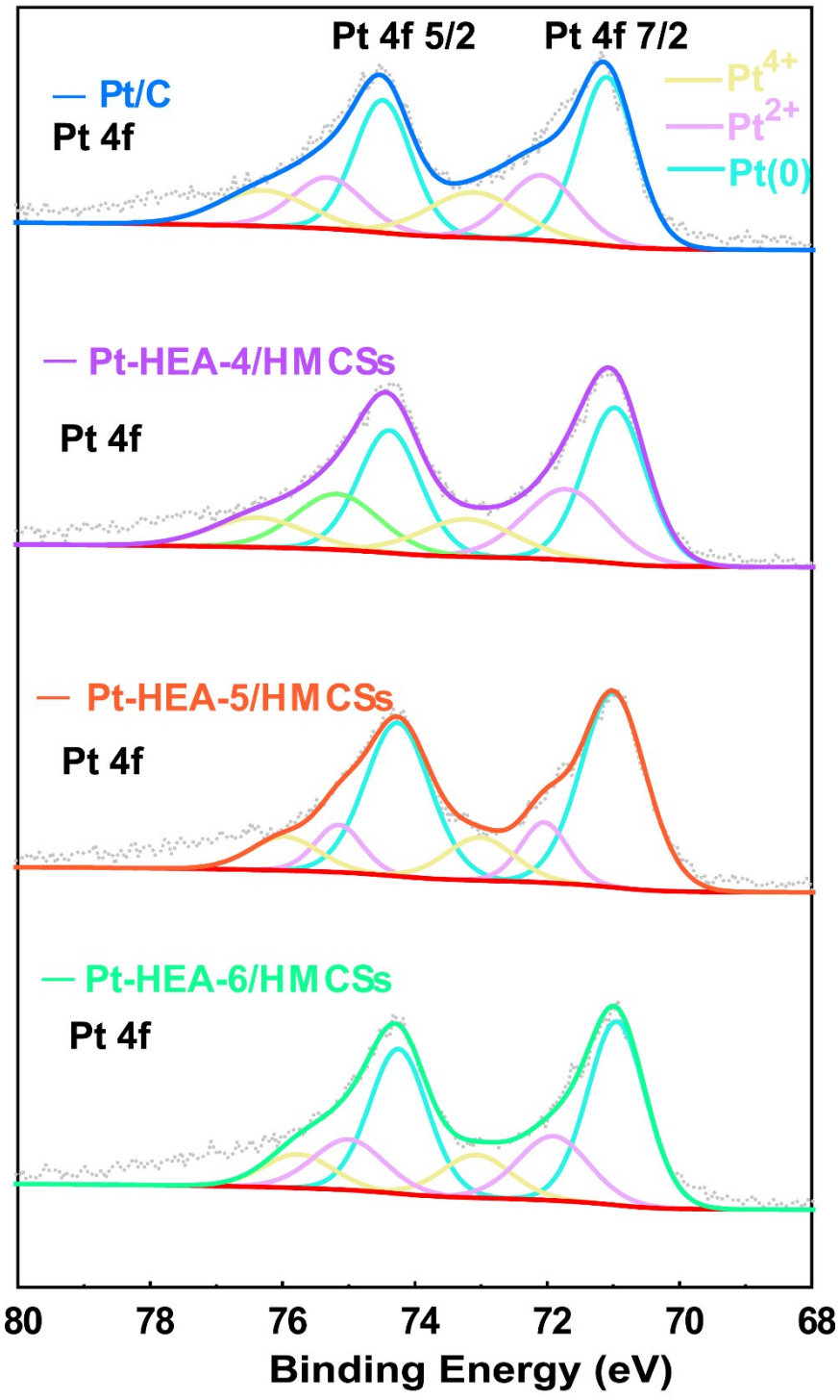

Figure S9. XPS spectra of Pt 4f for commercial Pt/C catalyst, Pt-HEA-4/HMCSs, Pt-HEA-5/HMCSs and Pt-HEA-6/HMCSs samples.

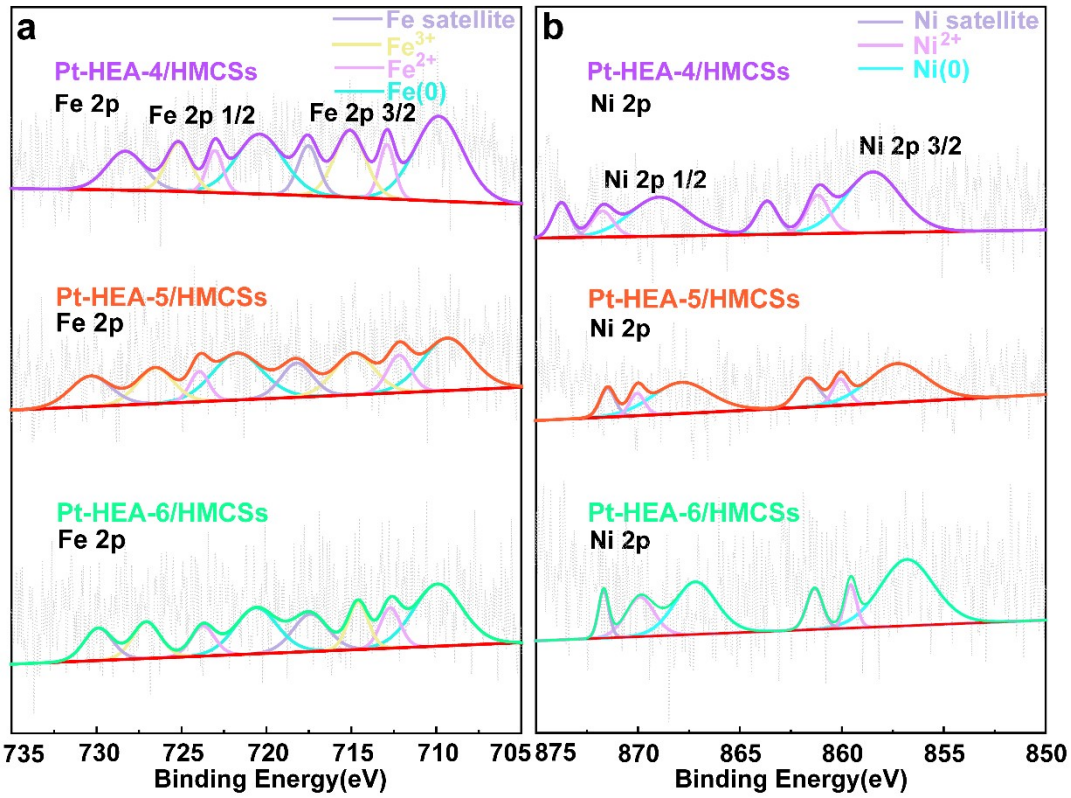

Figure S10. The XPS spectra of Fe 2p (a) and Ni 2p (b) for Pt-HEA-4/HMCSs, Pt-HEA-5/HMCSs and Pt-HEA-6/HMCSs samples.

Figure S11. The XPS spectra of Cu 2p for Pt-HEA-4/HMCSs, Pt-HEA-5/HMCSs and Pt-HEA-6/HMCSs samples (a) and Co 2p for Pt-HEA-5/HMCSs and Pt-HEA-6/HMCSs samples (b).

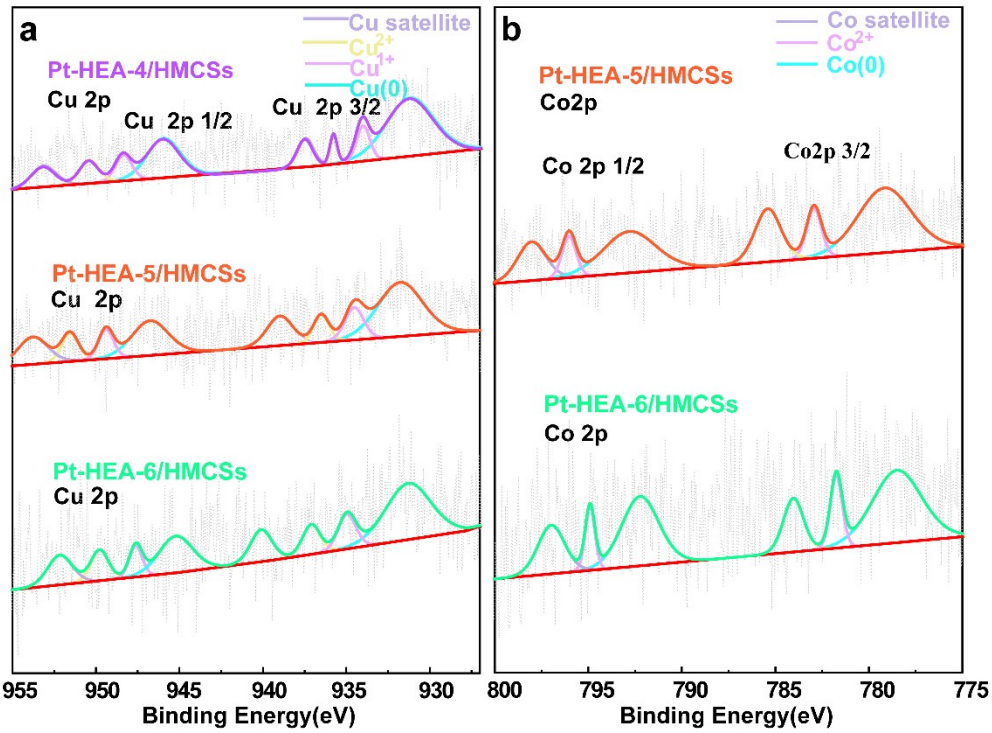

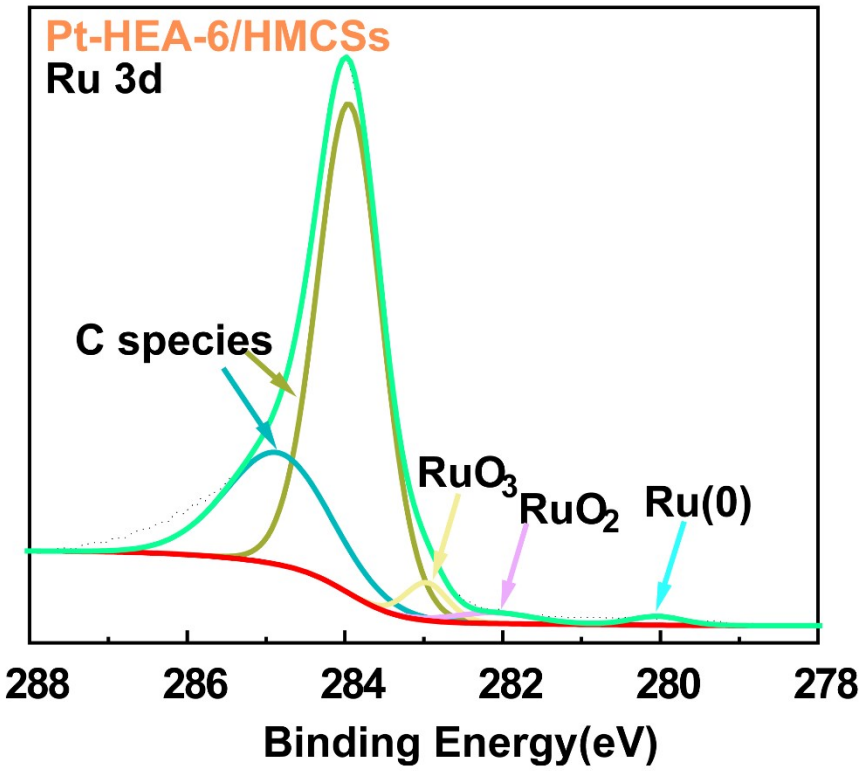

Figure S12. The XPS spectra of Ru 3d Pt-HEA-6/HMCSs.

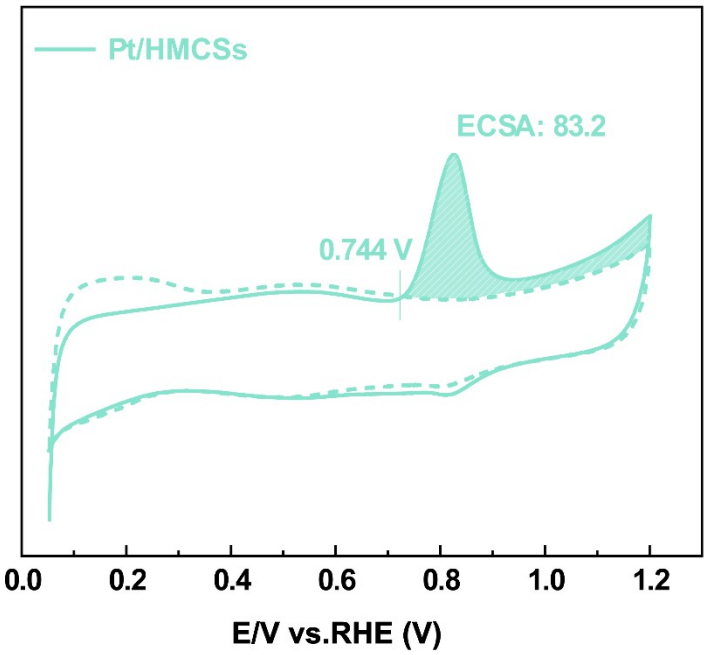

Figure S13. The CO stripping voltammograms of Pt/HMCSs in 0.1 mol L^{-1} $HClO_4$ solution at a scan rate of 30 mV s-1.

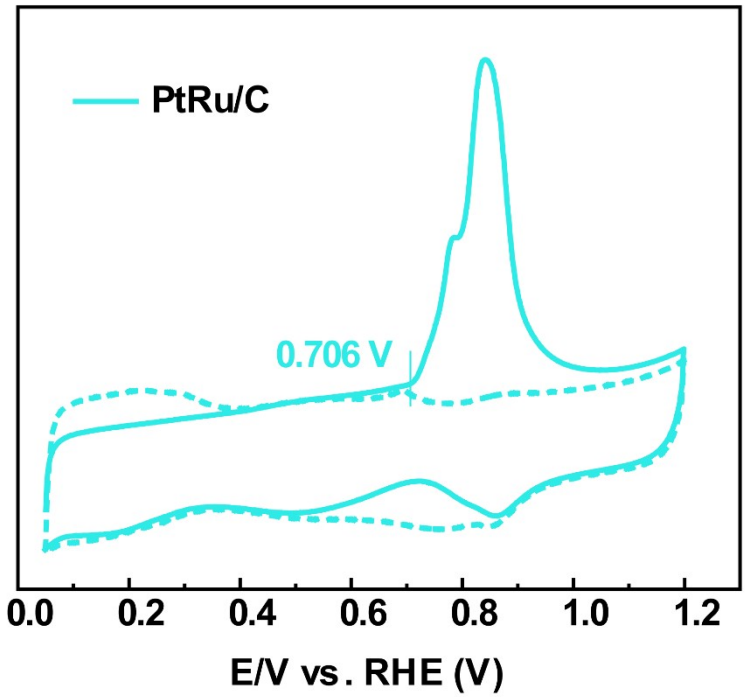

Figure S14. The CO stripping voltammograms of PtRu/C in 0.1 mol L^{-1} $HClO_4$ solution at a scan rate of 30 mV s-1.

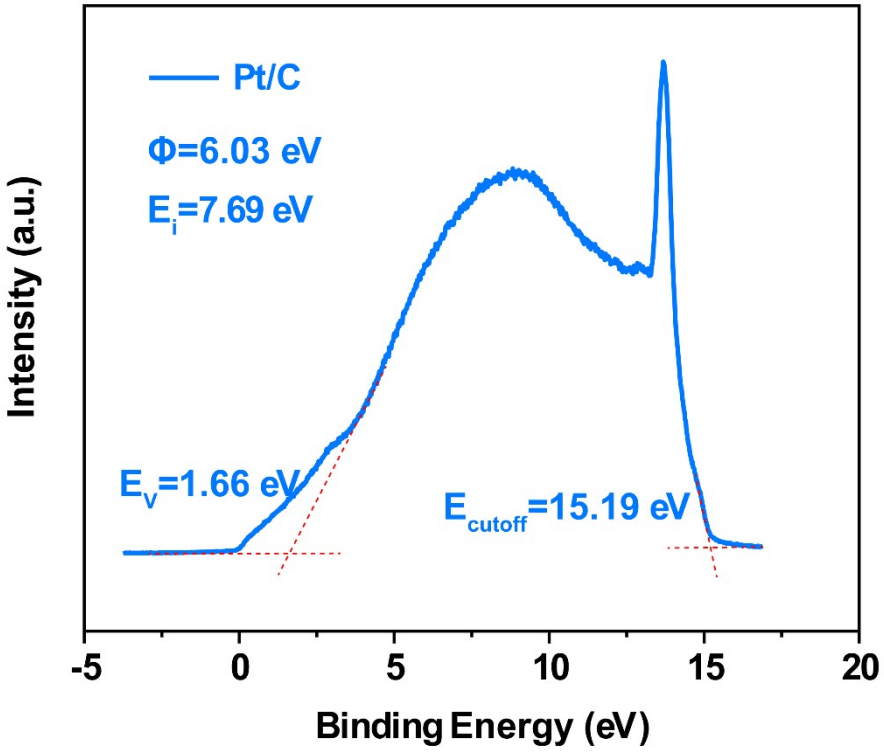

Figure S15. UPS spectra of P/C.

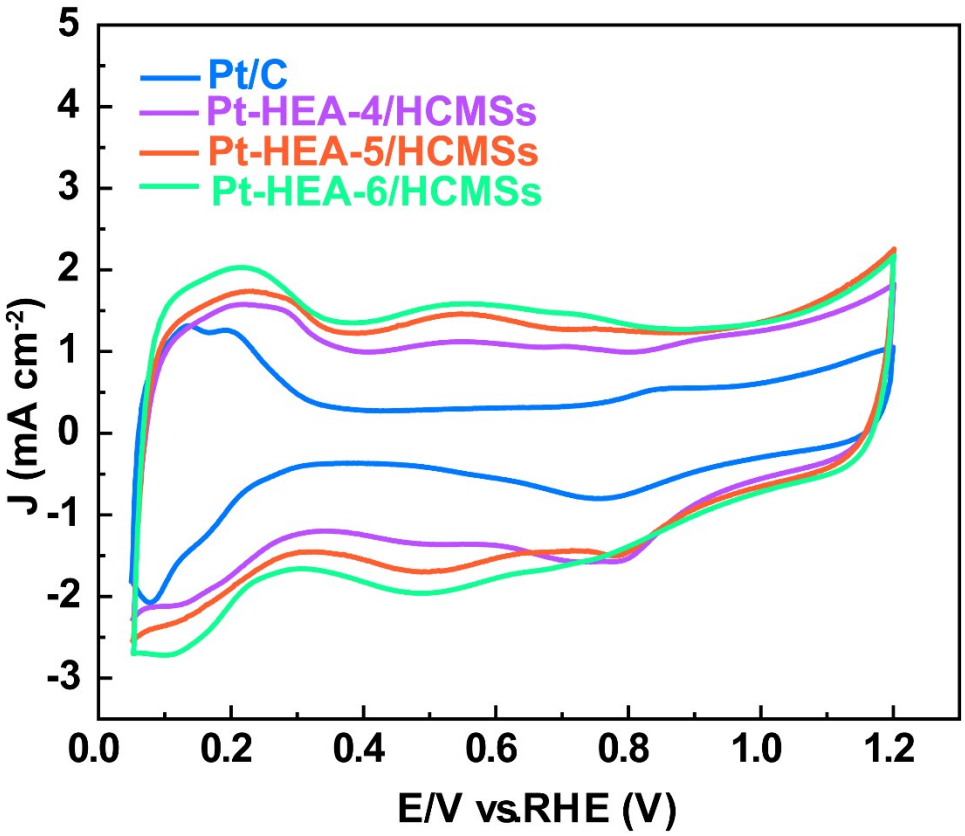

Figure S16. (a) Cyclic voltammograms of 0.1 M $HClO_4$ on the Pt/C, Pt-HEA-4/HMCSs, Pt-HEA-5/HMCSs and Pt-HEA-6/HMCSs catalysts at a scan rate of 50 mV s^{-1}.

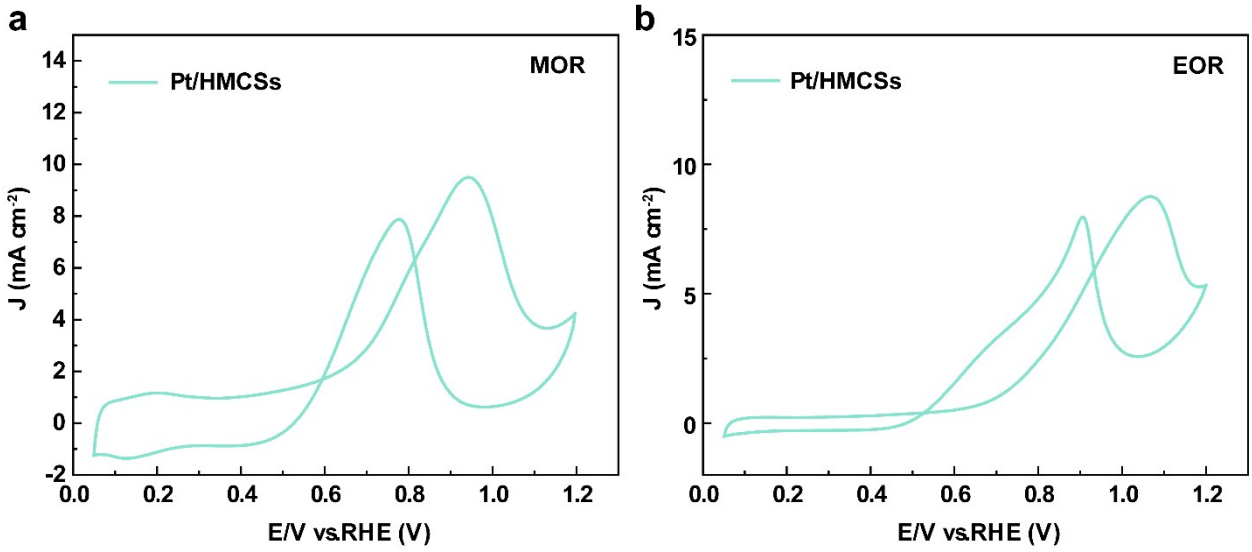

Figure S17. Cyclic voltammograms of (a) 0.5 M CH_3OH + 0.1 M $HClO_4$ and (b) 0.5

M CH_3CH_2OH + 0.1 M $HClO_4$ on the Pt/HMCSs at a scan rate of 50 mV s-1.

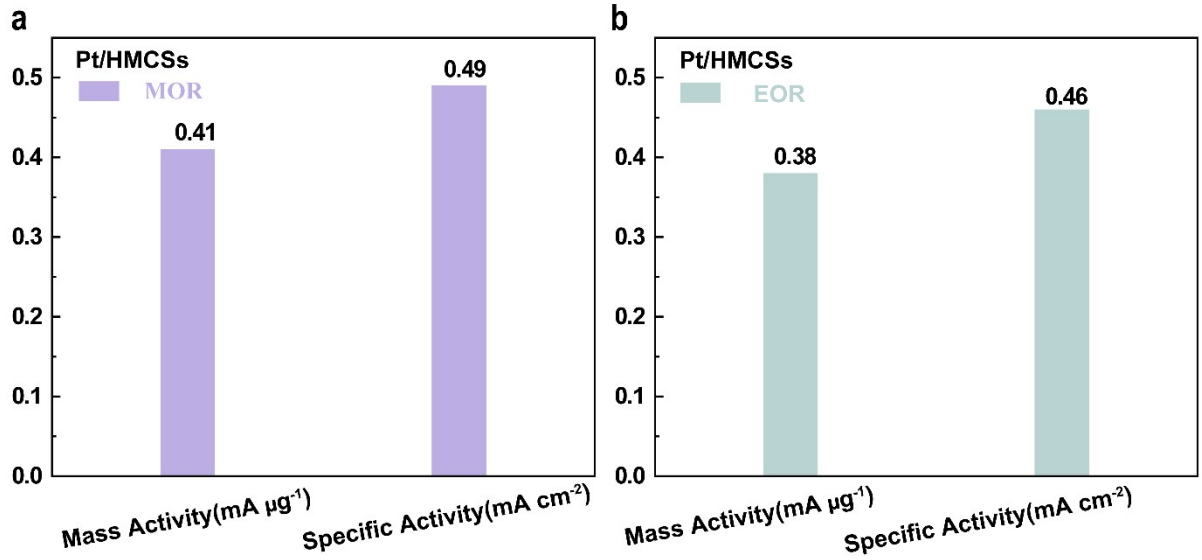

Figure S18. (a) The mass activity (MA) and specific activity (SA) of the Pt/HMCSs for MOR. (b) The mass activity (MA) and specific activity (SA) of the Pt/HMCSs for EOR.

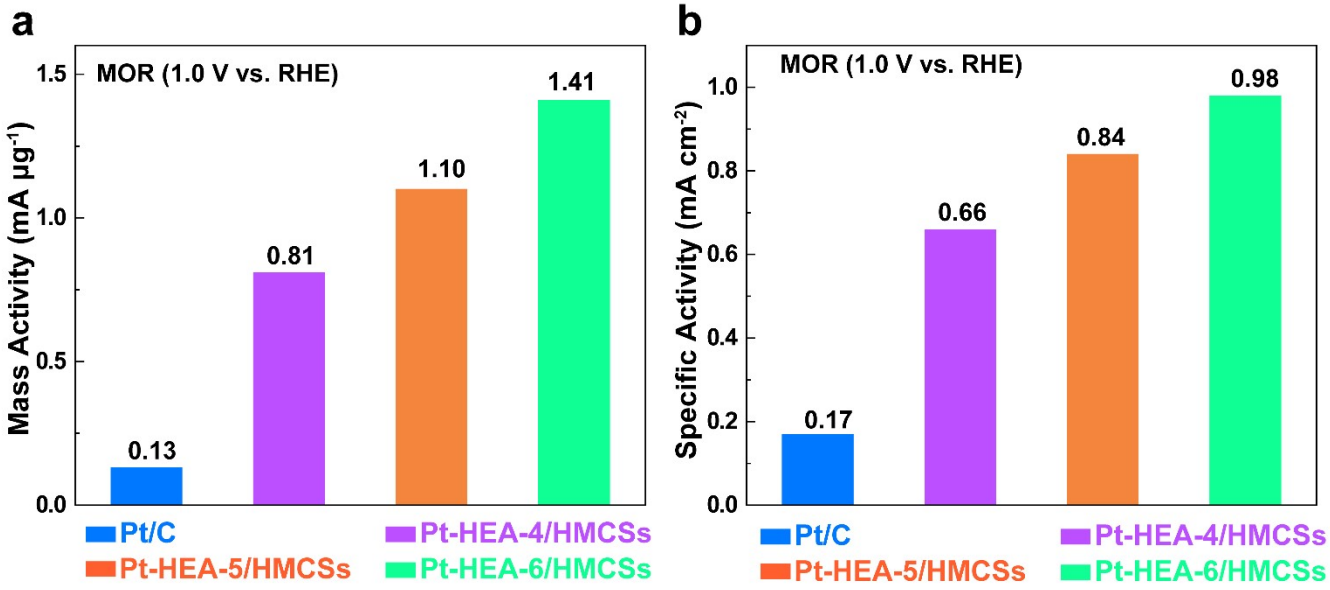

Figure S19. (a) MA and (b) SA at the 1.0 V vs. RHE.

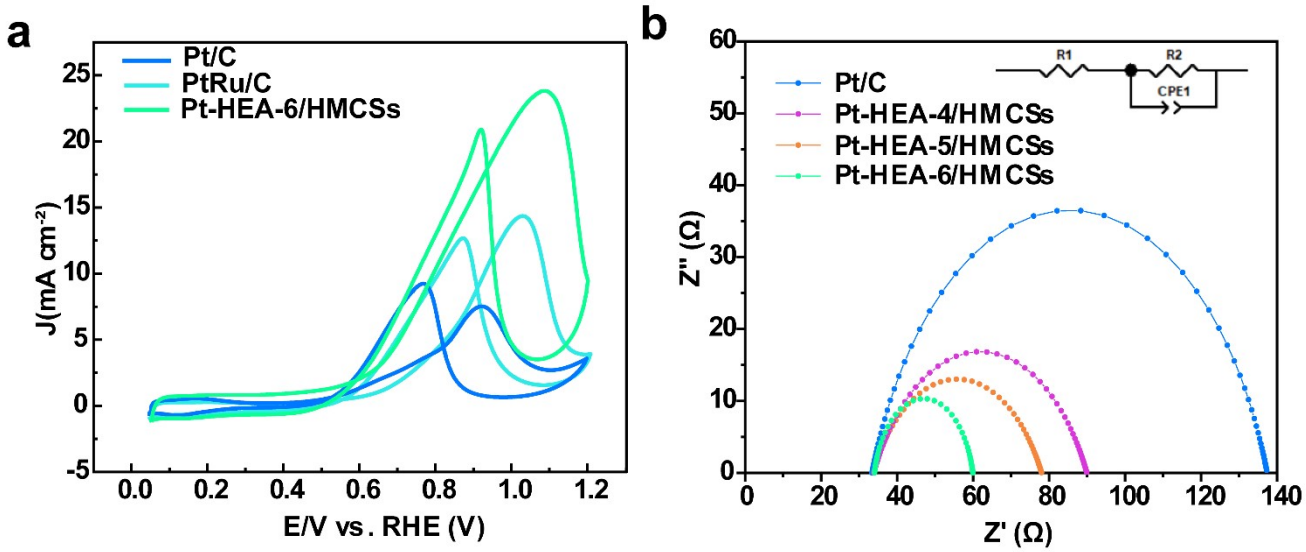

Figure S20. (a) Cyclic voltammograms of 0.5 M CH_3OH + 0.1 M $HClO_4$ on the Pt/C, PtRu/C and the Pt-HEA-6/HMCSs at a scan rate of 50 mV s-1, (b) The EIS diagrams of Pt/C, Pt-HEA-4/HMCSs, Pt-HEA-5/HMCSs and Pt-HEA-6/HMCSs.

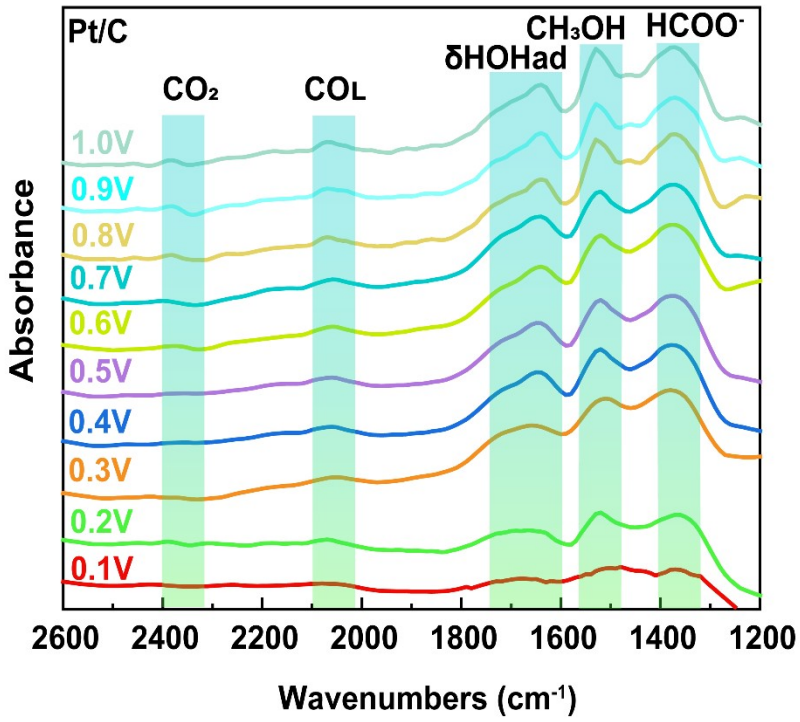

Figure S21. In situ FTIR spectra for methanol oxidation on commercial Pt/C catalyst.

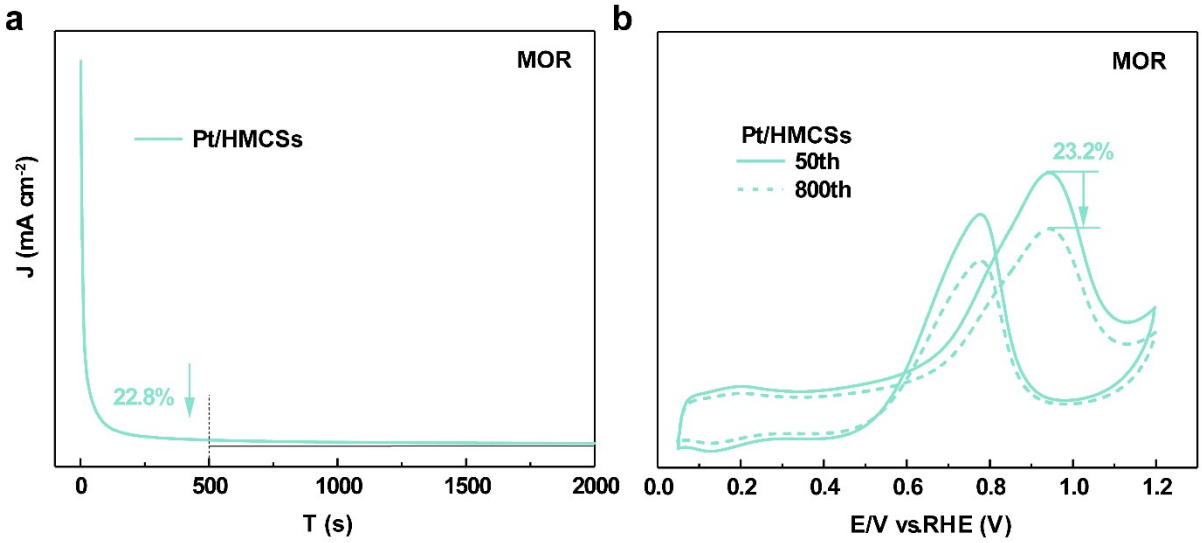

Figure S22. In N_2 saturated 0.1 M $HClO_4$ + 0.5 M CH_3OH solution, (a)chronoamperometric (CA) curves of Pt/HMCSs for 2000 s. (b) Cyclic voltammograms of Pt/HMCSs before and after 800 cycle durability tests at a scan rate of 50 mV s-1.

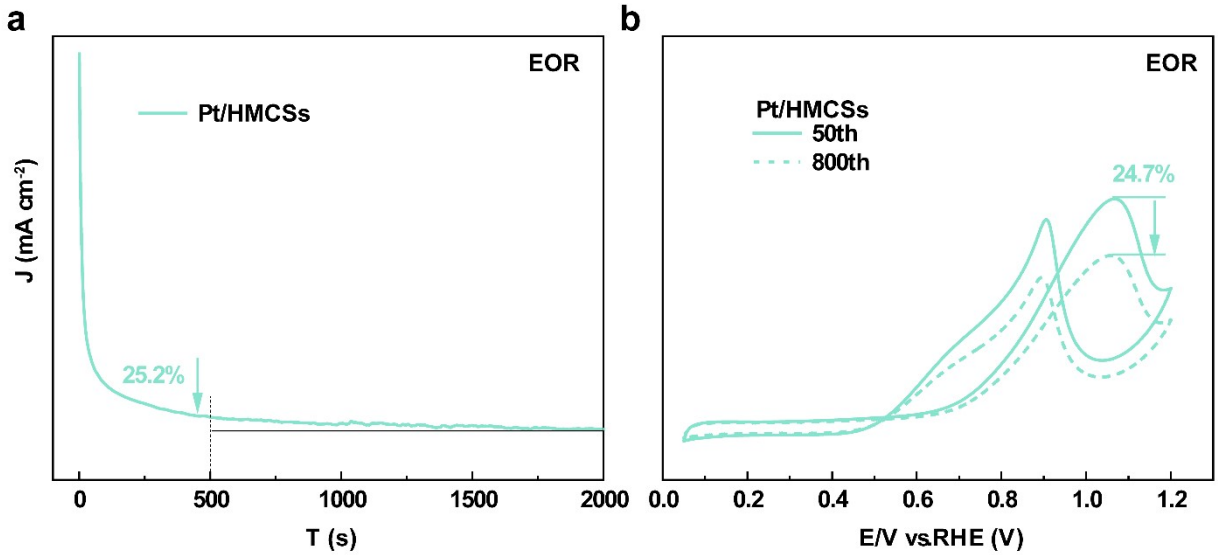

Figure S23. In N_2 saturated 0.1 M $HClO_4$ + 0.5 M CH_3CH_2OH solution, (a) chronoamperometric (CA) curves of Pt/HMCSs for 2000 s. (b) Cyclic voltammograms of Pt/HMCSs before and after 800 cycle durability tests at a scan rate of 50 mV s-1.

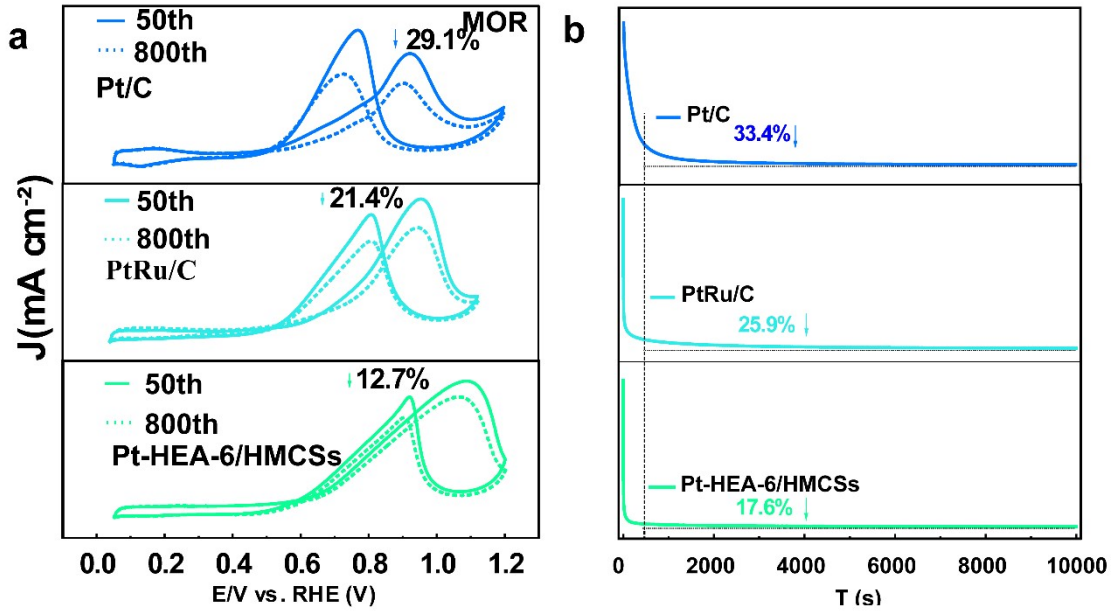

Figure S24. In N_2 saturated 0.1 M $HClO_4$ + 0.5 M CH_3OH solution, (a) Cyclic voltammograms of Pt/C, PtRu/C and Pt-HEA-6/HMCSs before and after 800 cycle durability tests at a scan rate of 50 mV s-1. (b) chronoamperometric (CA) curves of Pt/C, PtRu/C and Pt-HEA-6/HMCSs for10000 s.

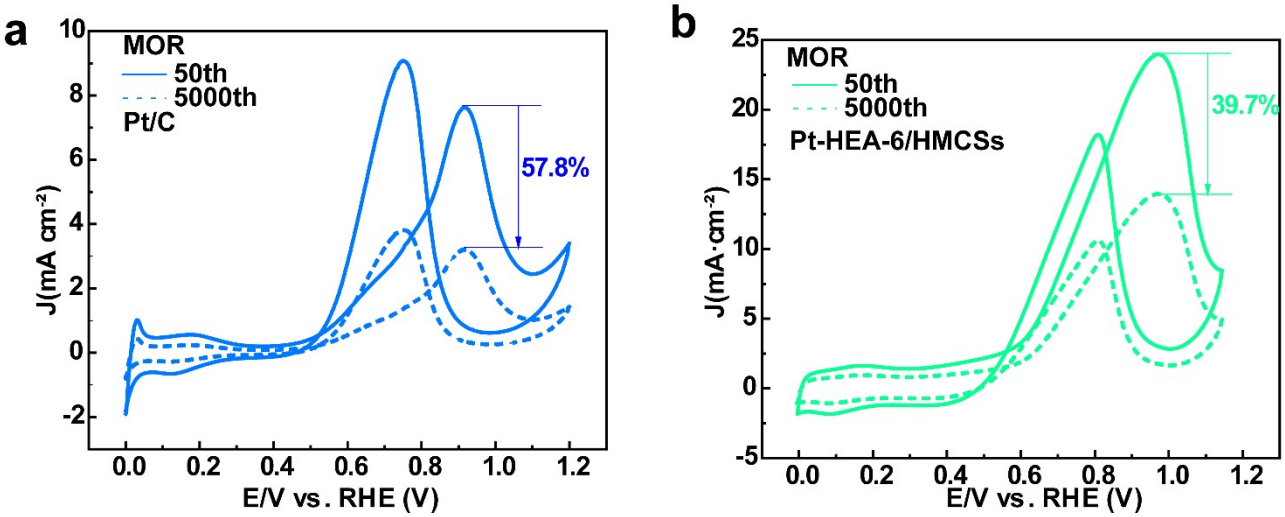

Figure S25. In N_2 saturated 0.1 M $HClO_4$ + 0.5 M CH_3OH solution, Cyclic voltammograms of (a) Pt/C and (b) Pt-HEA-6/HMCSs before and after 5000 cycle durability tests at a scan rate of 50 mV s-1.

Supplementary tables

Table S1. Lattice parameters and induced strain for Pt-HEA-4/HMCSs, Pt-HEA-5/HMCSs and Pt-HEA-6/HMCSs. based on XRD data.

Catalyst	2θ/degrees （111）	Lattice parameter （1/Å）	Strain (%)	I_{110}/I_{111}
Pt/C	39.770	0.2207	-	-
Pt-HEA-4/HMCSs	40.923	0.2269	2.81	0.33
Pt-HEA-5/HMCSs	41.115	0.2279	3.26	0.41
Pt-HEA-6/HMCSs	41.595	0.2305	4.44	0.43

Table S2. EXAFS fitting parameters at the Pt L_3-edge for various samples.

Sample	Path	CN	R (Å)	σ^2 (Å^2)	ΔE0 (eV)	R factor
Pt foil	Pt-Pt	12*	2.76±0.0038	0.0039±0.0005	7.01±0.63	0.010
Pt-HEA-6/HMCSs	Pt-Pt	6.85±0.23	2.68±0.0172	0.0090±0.0012	7.37±0.59	0.011
	Pt-M	4.39±0.35	2.61±0.0107	0.0127±0.0023		
PtO_2	Pt-O	5.68±0.46	2.01±0.0246	0.0034±0.0033	10.24±0.42	0.011

Table S3. XPS spectrum content for various samples.

Catalysts	Name							
	C1s (Wt%)	**O1s (Wt%)**	**Pt4f (Wt%)**	**Fe2p (Wt%)**	**Ni2p (Wt%)**	**Cu2p (Wt%)**	**Co2p (Wt%)**	**Ru3d (Wt%)**
Pt/C	76.31	5.04	18.65	-	-	-	-	-
Pt-HEA-4/HMCSs	84.65	5.20	7.85	1.14	0.56	0.60	-	-
Pt-HEA-5/HMCSs	85.04	4.77	6.48	1.19	0.75	0.64	1.13	-
Pt-HEA-6/HMCSs	85.26	4.71	6.17	1.22	0.72	0.51	1.07	0.34

Table S4. The elemental atomic loadings of Pt-HEA-4/HMCSs, Pt-HEA-5/HMCSs and Pt-HEA-6/HMCSs catalysts by using ICP.

Catalysts	ICP Loading by Atomic%					
	Pt loading (At%)	**Fe loading (At%)**	**Ni loading (At%)**	**Cu loading (At%)**	**Co loading (At%)**	**Ru loading (At%)**
Pt-HEA-4/HMCSs	49.71	19.50	17.59	13.20	-	-
Pt-HEA-5/HMCSs	43.01	16.07	12.22	11.42	16.48	-
Pt-HEA-6/HMCSs	39.71	15.67	12.40	10.61	14.53	7.08

Table S5. The elemental weight loadings of Pt-HEA-4/HMCSs, Pt-HEA-5/HMCSs and Pt-HEA-6/HMCSs catalysts by using ICP.

Catalysts	ICP Loading by Weight%					
	Pt loading (Wt%)	Fe loading (Wt%)	Ni loading (Wt%)	Cu loading (Wt%)	Co loading (Wt%)	Ru loading (Wt%)
Pt-HEA-4/HMCSs	76.34	8.65	8.33	6.68	-	-
Pt-HEA-5/HMCSs	71.15	8.19	6.13	6.23	8.30	-
Pt-HEA-6/HMCSs	66.76	7.55	6.28	5.85	7.38	6.18

Table S6. The elemental loadings of Pt-HEA-4/HMCSs, Pt-HEA-5/HMCSs and Pt-HEA-6/HMCSs catalysts by weight percent of Pt, Fe, Ni, Cu, Co and Ru using ,by EELS line scan and XPS.

Catalysts	ICP Loading by Weight%			EELS line scan Loading by Weight%			XPS Loading by Weight%		
	Pt-HEA-4/HMCSs			Pt-HEA-5/HMCSs			Pt-HEA-6/HMCSs		
Pt	76.34	-	77.34	71.15	-	63.59	66.76	75.41	61.52
Fe	8.65	-	11.23	8.19	-	11.67	7.55	6.46	12.16
Ni	8.33	-	5.52	6.13	-	7.36	6.28	3.79	7.18
Cu	6.68	-	5.91	6.23	-	6.29	5.85	4.29	5.08
Co	-	-	-	8.30	-	11.09	7.38	6.24	10.67
Ru	-	-	-	-	-	-	6.18	3.81	3.39

Table S7. Pt loading and, $ECSA_{CO}$, mass activity and specific activity, forward peak current, onset potential, I_f/I_b in 0.1 M $HClO_4$ + 0.5 M CH_3OH solution for various samples.

Catalysts	Pt loading (μg)	ECSA (m^2/g)	Mass activity ($mA/\mu g_{Pt}$)	Specific activity (mA/cm^2)	Forward peak current ($j/mA/cm^2$)	Onset potential (V)	I_f/I_b
Pt/C	6.21	77.8	0.24	0.31	7.55	0.43	0.82
Pt-HEA-4/HMCSs	3.39	122.6	0.83	0.68	14.34	0.42	1.23
Pt-HEA-5/HMCSs	3.24	130.7	1.17	0.90	19.24	0.38	1.17
Pt-HEA-6/HMCSs	3.05	144.5	1.54	1.07	23.93	0.33	1.18
Pt/HMCSs	4.57	83.2	0.41	0.49	9.58	0.43	1.22

Table S8. Pt loading and, $ECSA_{CO}$, mass activity and specific activity, forward peak current, onset potential, I_f/I_b in 0.1 M $HClO_4$ + 0.5 M CH_3CH_2OH solution for various samples.

Catalysts	**Pt loading (μg)**	**ECSA (m^2/g)**	**Mass activity ($mA/\mu g_{Pt}$)**	**Specific activity (mA/cm^2)**	**Forward peak current ($j/mA/cm^2$)**	**Onset potential (V)**	**I_f/I_b**
Pt/C	6.21	77.8	0.29	0.37	9.23	0.51	1.09
Pt-HEA-4/HMCSs	3.39	122.6	0.71	0.58	12.24	0.39	0.99
Pt-HEA-5/HMCSs	3.24	130.7	1.01	0.77	16.63	0.34	1.15
Pt-HEA-6/HMCSs	3.05	144.5	1.26	0.87	19.55	0.31	1.03
Pt/HMCSs	4.57	83.2	0.38	0.46	8.78	0.48	1.19

Table S9. Comparisons of the MOR performance of Pt-HEA-6/HMCSs and other recently reported Pt-based electrocatalysts.

Catalysts	**Mass activity ($mA/\mu g_{pt}$)**	**Electrolyte**	**Reference**
Pt_3Pd_1/CeO_2	0.85	0.1 M H_2SO_4 + 1.0 M CH_3OH	[1]
$Pt/CeO_2/CNTs$	0.63	1.0 M $HClO_4$ + 1.0 M CH_3OH	[2]
PtBi nanoplates	1.10	0.5 M H_2SO_4 + 1 M CH_3OH	[3]
PtZn/MWNT	0.61	0.5 M H_2SO_4 + 1 M CH_3OH	[4]
Cu-$Pt_{5.2}Ru_1$	0.64	0.5 M H_2SO_4 + 1.0 M CH_3OH	[5]
PEDOT/DLHCs/Pt	0.81	0.5 M H_2SO_4 + 1 M CH_3OH	[6]
$Pd_{52}Pt_{48}$ Nanodendrites	0.83	0.1 M $HClO_4$+ 1 M CH_3OH	[7]
PtRuFe Nanodendrities	1.14	0.5 M H_2SO_4 + 1.0 M CH_3OH	[8]
$Pt_1Cu_1Co_1Ni_1$ NPQAs	0.45	0.5 M H_2SO_4 + 0.5 M CH_3OH	[9]
Pt nanowires	0.34	0.5 M H_2SO_4 + 1 M CH_3OH	[10]
Pt-HEA-6/MWCNTs	1.**5**4	0.1 M $HClO_4$+ 0.5M CH_3OH	This work

Table S10. The precursor solution of the prepared sample and its concentration.

Catalysts	Precursor solution					
Pt/HMCSs	$H_2PtCl_6.6H_2O$ (19.75 mg/mL) 865 μL	-	-	-	-	-
Pt-HEA-4/HMCSs	$H_2PtCl_6.6H_2O$ (19.75 mg/mL) 865 μL	$Fe(NO_3)_3·6H_2O$ (0.5 M) 200 μL	$NiCl_2$ (0.1 M) 200 μL	$CuSO_4$ (0.1 M) 200 μL	-	-
Pt-HEA-5/HMCSs	$H_2PtCl_6.6H_2O$ (19.75 mg/mL) 865 μL	$Fe(NO_3)_3·6H_2O$ (0.5 M) 200 μL	$NiCl_2$ (0.1 M) 200 μL	$CuSO_4$ (0.1 M) 200 μL	$Co(NO_3)_2·6H_2O$ (0.5 M) 200 μL	-
Pt-HEA-6/HMCSs	$H_2PtCl_6.6H_2O$ (19.75 mg/mL) 865 μL	$Fe(NO_3)_3·6H_2O$ (0.5 M) 200 μL	$NiCl_2$ (0.1 M) 200 μL	$CuSO_4$ (0.1 M) 200 μL	$Co(NO_3)_2·6H_2O$ (0.5 M) 200 μL	$RuCl_3$, (18.15 mg/mL) 200 μL

References

[1] A.B. Yousaf, M. Imran, N. Uwitonze, A. Zeb, S.J. Zaidi, T.M. Ansari, G. Yasmeen, S. Manzoor, Enhanced electrocatalytic performance of Pt_3Pd_1 alloys supported on CeO_2/C for methanol oxidation and oxygen reduction reactions, J. Phys. Chem. C, 2017, 121, 2069-2079.

[2] J. Wang, J. Xi, Y. Bai, Y. Shen, J. Sun, L. Chen, W. Zhu, X. Qiu, Structural designing of Pt-CeO_2/CNTs for methanol electro-oxidation, J. Power Sources, 2007, 164, 555-560.

[3] Y. Qin, M. Luo, Y. Sun, C. Li, B. Huang, Y. Yang, Y. Li, L. Wang, S. Guo,

Intermetallic hcp-PtBi/fcc-Pt Core/Shell nanoplates enable efficient bifunctional oxygen reduction and methanol oxidation electrocatalysis, ACS Catal. 2018, 8, 5581-5590.

[4] Z. Qi, C. Xiao, C. Liu, T.W. Goh, L. Zhou, R. Maligal-Ganesh, Y. Pei, X. Li, L.A. Curtiss, W. Huang, Sub-4 nm PtZn intermetallic nanoparticles for enhanced mass and specific activities in catalytic electrooxidation reaction, J. Am. Chem. Soc. 2017, 139, 4762-4768.

[5] W. Zhou, R. Yan, S. Zhou, Synthesis of highly efficient Cu-PtRu ternary metal catalyst for methanol oxidation, Surf. Interfaces, 2023, 40, 103131.

[6] M. Niyaz, N. Sawut, R. Jamal, T. Abdiryim, Z. Helil, H. Liu, S. Xie, Y. Song, Preparation of PEDOT-modified double-layered hollow carbon spheres as Pt catalyst support for methanol oxidation, Int. J. Hydrogen Energy, 2021, 46, 31623-31633.

[7] Y. Zhang, J. Zhang, Z. Chen, Y. Liu, M. Zhang, X. Han, C. Zhong, W. Hu, Y. Deng, One-step synthesis of the PdPt bimetallic nanodendrites with controllable composition for methanol oxidation reaction, Sci. China Mater. 2018, 61, 697-706.

[8] Z. Cai, Y. Kuang, X. Qi, P. Wang, Y. Zhang, Z. Zhang, X. Sun, Ultrathin branched PtFe and PtRuFe nanodendrites with enhanced electrocatalytic activity, J. Mater. Chem. A, 2015, 3, 1182-1187.

[9] S. Fu, C. Zhu, D. Du, Y. Lin, Enhanced electrocatalytic activities of PtCuCoNi Three-Dimensional nanoporous quaternary alloys for oxygen reduction and methanol oxidation reactions, ACS Appl. Mater. Interfaces, 2016, 8, 6110-6.

[10] J. Liu, Z. Liu, H. Wang, B. Liu, N. Zhao, C. Zhong, W. Hu, Designing nanoporous Coral-Like Pt nanowires architecture for methanol and ammonia oxidation reactions, Adv. Funct. Mater. 2022, 32, 2110702.